

Predicting lesion size by accumulated thermal dose in MR-guided focused ultrasound for essential tremor

Yuexi Huang^{a)}

Physical Sciences, Sunnybrook Research Institute, 2075 Bayview Avenue, Toronto, ON M4N 3M5, Canada

Nir Lipsman and Michael L. Schwartz

Division of Neurosurgery, Sunnybrook Health Sciences Centre, 2075 Bayview Avenue, Toronto, ON M4N 3M5, Canada

Vibhor Krishna, Francesco Sammartino, and Andres M. Lozano

Division of Neurosurgery, Toronto Western Hospital, 399 Bathurst Street, Toronto, ON M5T 2S8, Canada

Kullervo Hynynen

Physical Sciences, Sunnybrook Research Institute, 2075 Bayview Avenue, Toronto, ON M4N 3M5, Canada

Department of Medical Biophysics, University of Toronto, 101 College Street, Toronto, ON M5G 1L7, Canada

(Received 5 October 2017; revised 23 July 2018; accepted for publication 6 August 2018; published 31 August 2018)

Purpose: To correlate the accumulated thermal dose (ATD) with lesion size in magnetic resonance (MR)-guided focused ultrasound (MRgFUS) thalamotomy to help guide future clinical treatments.

Materials and Methods: Thirty-six patients with medication-refractory essential tremor were treated using a commercial MRgFUS brain system (ExAblate 4000, InSightec) in a 3T MR scanner (MR750, GE Healthcare). Intraoperative MR-thermometry was performed to measure the induced temperature and thermal dose distributions (thermal coefficient = -0.00909 ppm/°C). The ATD was calculated over multiple sonications with appropriate corrections for spatial-shifting artifacts. The ATD profile sizes obtained for dose values of 17, 40, 100, 200, and 240 cumulative equivalent minutes at 43°C (CEM) were correlated with the corresponding lesion sizes measured via axial T1- and T2-weighted MR images acquired 1 day post-treatment.

Results: Of a total of 232 included sonications, 83 required corrections for off-resonance-induced spatial-shifting artifacts (correction range = [1.1,2.2] mm). The mean lesion sizes measured on T2-weighted MR images (6.2 ± 1.3 mm, mean \pm SD) were 15% larger than those measured on corresponding T1-weighted MR images (5.3 ± 1.2 mm, mean \pm SD). The ATD values that provided the best correlations with the measured lesion sizes on T2- and T1-weighted MR images were 100 and 200 CEM, respectively.

Conclusion: The ATD was correlated with lesion size measured 1 day following MRgFUS thalamotomy for essential tremor. These data provide useful information for predicting brain lesion size and determining treatment endpoints in future clinical MRgFUS procedures. © 2018 American Association of Physicists in Medicine [https://doi.org/10.1002/mp.13126]

Key words: accumulated thermal dose, high-intensity focused ultrasound, MR-thermometry, thermal ablation, thermal dose

1. INTRODUCTION

Thalamotomy by magnetic resonance (MR)-guided focused ultrasound (MRgFUS) was recently approved by the U.S. Food and Drug Administration for the treatment of essential tremor following demonstration of the procedure's efficacy and safety profiles in a randomized, controlled, multicenter clinical trial.¹ The procedure involves creating a thermal lesion in the ventral intermediate (VIM) nucleus of the thalamus [Fig. 1(a)], which in turn suppresses the transmission of tremor signals between the cerebellar input and the motor cortex. Initial results from this randomized clinical trial demonstrated a mean improvement in hand tremor score of 47% in the thalamotomy group 3 months post-treatment, compared to 0.1% in the sham-procedure group at the same time point.¹ In contrast to deep-brain stimulation, the current surgical standard that involves the

insertion of electrodes into the brain and the implantation of neurostimulators/batteries, MRgFUS offers an alternative incisionless treatment option to patients with essential tremor.

The applied acoustic energy required to produce a lesion in the brain via MRgFUS varies substantially from patient-to-patient.¹⁻⁴ Intraoperative MR imaging is thus not only important from an anatomical targeting perspective, but is also critical for monitoring the induced temperature distributions to help ensure consistent clinical outcomes.⁵ Clinical experience has shown that although precise targeting of the VIM nucleus is required to induce immediate therapeutic effects (i.e., tremor suppression), the production of an appropriately sized lesion is also important to achieve durable efficacy.⁶ Thermal brain lesions generated via MRgFUS tend to grow in size until several hours or days after the treatment.⁷ It would therefore be useful if thermal dose data based on

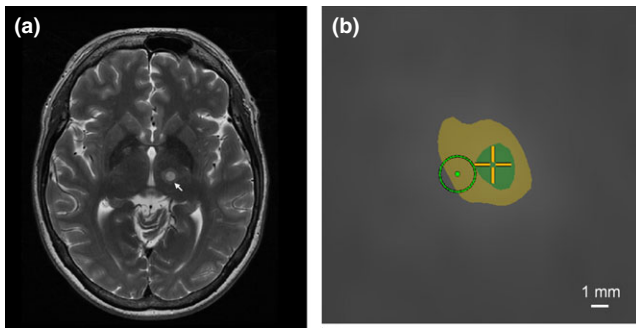


FIG. 1. (a). Axial T2-weighted MR image acquired 1 day post-treatment showing a lesion in the VIM nucleus (arrow); (b). Screenshot from the MRgFUS system console displaying a thermal dose calculation after a single sonication in the same patient (axial plane, zoomed in around the target). The green (inner) and yellow (outer) areas represent regions that received a thermal dose exceeding 240 and 17 CEM, respectively. The light green circle denotes the intended target zone (diameter ~ 2 mm). In this example, the frequency encoding direction was left-to-right, and an off-resonance-induced shift on the order of 2 mm was observed along this direction. [Color figure can be viewed at wileyonlinelibrary.com]

intraoperative MR-thermometry could be used to predict the ultimate lesion size, and thus better define clinical treatment endpoints.

Previous studies in animal models have established a range of thermal dose values for estimating the size of lesions produced in brain tissue via MRgFUS, namely between 17 and 240 cumulative equivalent minutes (CEM) at 43°C .^{8,9} A preliminary study on clinical data from essential tremor treatments conducted at our institution confirmed this range using the highest energy sonication as the dominant thermal dose statistic.¹⁰ However, in many patient treatments, sonications with similar peak temperature elevations are repeated multiple times to enlarge the overall lesion size and consolidate the tremor suppression outcome, either with or without adjusting the target location based on patient feedback. In these cases, a more appropriate measure of the total thermal dose would be obtained by integrating the thermal dose from each individual sonication over the entire treatment to obtain the accumulated thermal dose (ATD). However, proper calculation of the ATD during clinical MRgFUS treatments raises several technical challenges. For instance, because MR-thermometry is typically carried out in multiple orthogonal two-dimensional planes (i.e., axial, coronal, sagittal) throughout the procedures using different frequency encoding directions and a fixed center frequency, spatial misalignments of the measured heating areas can arise due to artifacts caused by off-resonance.¹¹ A PubMed search performed on Oct 5 2017 with the terms: “accumulated thermal dose”, “human,” and “brain” suggested that no data regarding the ATD required for *in vivo* brain tissue ablation in humans have been reported to date.

In this work, corrections for off-resonance-induced spatial-shifting artifacts were performed retrospectively on a sonication-by-sonication basis for assessment of the ATD during clinical MRgFUS treatments of essential tremor. Lesion size measurements made on both T1- and T2-weighted MR images 1 day post-treatment were compared to the corresponding ATD profile sizes at various dose values. This study

aimed to establish the ATD thresholds for *in vivo* human brain tissue ablation via MRgFUS, data that were previously lacking in the literature, to provide practical information for predicting lesion size and determining treatment endpoints in clinical practice.

2. MATERIALS AND METHODS

Thirty-six patients with medication-refractory essential tremor were treated at our institution (Sunnybrook Research Institute, Toronto, ON, Canada) using a commercial MRgFUS brain system (ExAblate 4000, 650 kHz center frequency, 1024 transducer elements, InSightec, Tirat Carmel, Israel) in a 3T MR scanner (MR750, GE Healthcare, Milwaukee, WI, USA) between May 2012 and October 2016. Patients were configured within the MRgFUS array using a stereotactic frame as described previously.² A computed tomography (CT)-based focusing algorithm was applied to correct for the ultrasound beam aberrations induced by the intact skull bone.¹²

Since the VIM nucleus could not be directly observed via standard MRI sequences, distance measurements from anatomical landmarks (i.e., the anterior and posterior commissures) were used for the initial estimate of the target based on the global average location documented from previous clinical experience.¹³ Initially, low-power sonications were performed to raise the target temperature to approximately 45°C for alignment of the focal heating volume based on MR-thermometry. The magnitude of the applied acoustic power and duration of heating varied substantially between different patients, ranging from 150 to 500 W over a period of 10–17 s. The dominant factor causing this variability was likely the different skull properties (e.g., thickness, density, uniformity) between patients. The applied acoustic power and sonication duration for a given patient were adjusted based on the peak focal temperature obtained via MR-thermometry, which reduced the variability observed in the treatment effectiveness substantially compared to the previous approach of using fixed values for the applied acoustic power/sonication duration. Following this initial targeting step, the applied acoustic power and/or sonication duration were gradually increased to raise the peak focal temperature to approximately 50°C , which is below the threshold required to produce a permanent lesion yet capable of causing transient sensations from adjacent sensory nuclei, information that can be used as feedback from the awake patient to adjust the target location.^{2,3} The duration of the adjustment period typically lasted between 30 min and 1 h. Once the target location was confirmed in the absence of any unwanted side effects, the applied acoustic power and sonication duration were further increased to raise the focal temperature to 55 – 60°C degrees to form a permanent lesion. The ability to spatially map the induced temperature distributions intraoperatively and to receive sensory feedback at intermediate temperatures provide improved levels of confidence regarding anatomical targeting during MRgFUS procedures relative to Gamma Knife radiosurgery, an alternative noninvasive treatment option.²

Two-dimensional MR-thermometry [repetition time (TR) = 27.6 ms, echo time (TE) = 12.8 ms, slice thickness = 3 mm, field of view (FOV) = 28 × 28 cm, matrix size = 256 × 128 zero padded to 256 × 256, in-plane resolution = 1.1 mm, temporal resolution = 3.5 s, bandwidth = 44 Hz/pixel] was applied separately in three orthogonal planes (i.e., axial, coronal, and sagittal) to measure the induced temperature and thermal dose distributions. The MRgFUS system software used a thermal coefficient of -0.00909 ppm/°C to calculate the thermal maps, and all images were acquired using the MRI system's built-in body coil. A low bandwidth (44 Hz/pixel) was applied to improve upon the low signal-to-noise ratio (SNR) provided by the body coil. However, the use of such a low bandwidth increased off-resonance-induced spatial shifting in the frequency encoding direction. The dominant sources of these artifacts were magnetic susceptibility-induced off-resonance caused by the presence of approximately 5 L of degassed water between the patient's head and the ultrasound transducer array, as well as the need for a fixed center frequency across all axial, coronal, and sagittal images for proper three-dimensional spatial registration. Although the center frequency was individually optimized at the beginning of each treatment using a multiecho gradient echo sequence for field mapping, the magnitude of these off-resonance-induced shifts were still on the order of 1–2 mm. To ensure accurate targeting during the treatments, two-dimensional MR-thermometry was carried out in orthogonal planes (i.e., axial, coronal, and sagittal) using different frequency-encoding directions; each plane provided information regarding the focal heating alignment along the phase-encoding direction, in which no spatial-shifting artifact was present. This alignment procedure normally consists of three consecutive sonications: (a) axial imaging with LR as the phase-encoding direction to verify and correct alignment on LR. Any misalignment along the frequency-encoding direction (AP in this case) was assumed to be a result of spatial-shifting artifacts and therefore ignored; (b) axial imaging with AP as the phase-encoding direction to verify and correct alignment on AP (misalignment on LR was ignored); and (c) coronal imaging with SI as the phase-encoding direction to verify and correct alignment on SI (misalignment on LR was ignored). Based on the above procedure, the center of the heating volume was assumed to be aligned with the intended target before any high-power sonications were carried out. The targeting accuracy of the MRgFUS brain system employed in this work has been shown to be less than 1 mm.¹⁴ For each sonication, a misalignment of the heating area on the frequency-encoding direction was expected and ignored [Fig. 1(b)]. Although this misalignment was acceptable for monitoring temperature and thermal dose distributions from a given sonication, it resulted in a distortion of the ATD calculated across multiple sonications with different frequency-encoding directions. If the misalignment was found to be more than half of the pixel width (i.e., 0.5 mm), corrections were performed retrospectively in MATLABTM (The MathWorks, Inc., Natick, MA, USA) by shifting the image translationally along the

frequency encoding direction until the center of the heating volume in that direction was realigned with the target. Corrections were performed independently for each sonication. For example, if in one sonication the hotspot was 2 mm shifted to the left from the intended target, the entire set of thermometry images for that sonication was shifted to the right by 2 mm such that the hotspot was re-aligned with the target. If in another sonication the misalignment was found to be 1 mm, the entire set of thermometry images was shifted by 1 mm for that particular sonication. Following correction, the spatial misalignment should be at most 0.5 mm. Only sonications with a peak temperature greater than or equal to 50°C were considered in this work. Because the majority of MR-thermometry scans were performed in an axial plane (perpendicular to the transducer's acoustical axis), ATDs were calculated in an axial plane using the standard thermal dose model.^{15,16} For the subset of sonications in which MR-thermometry was performed either in a coronal or sagittal plane (14% of all sonications), the focal heating volume was assumed to be ellipsoidal in shape and was transformed into an axial plane by rotating the appropriate line profile about the center of the focus.

The ATD profile sizes at 17, 40, 100, 200, and 240 CEM were measured and correlated with lesion sizes obtained from T1- (3D FSPGR, TR = 8.3 ms, TE = 3.3 ms, slice thickness = 1.2 mm) and T2-weighted MR images (FRFSE, TR = 5200 ms, TE = 100 ms, slice thickness = 3 mm) acquired 1 day post-treatment. The ATD and lesion sizes represented maximum diameters, and were measured in the left-to-right and anterior-to-posterior dimensions independently. For the T1-weighted MR images, the lesion size was measured by the diameter of the hypointense region [Fig. 2(a)]. For the T2-weighted MR images, the lesion size included zones I and II as defined in Ref. [7] but excluded zone III, the latter of which represents vasogenic edema that is absorbed over time [Fig. 2(b)]. Paired *t*-tests with null hypotheses that on average the ATD sizes were equivalent to the lesion sizes measured on T1- or T2-weighted MR images were carried out using MATLABTM.

3. RESULTS

Of the 232 sonications included in this study, 83 required corrections for off-resonance-induced shifting artifacts. The spatial correction values ranged from 1 to 2 pixels, which corresponded to a size of 1.1–2.2 mm. The mean lesion size measured via axial T2-weighted MR images (6.2 ± 1.3 mm, mean \pm SD) was 15% larger than that found from corresponding T1-weighted MR images (5.3 ± 1.2 mm, mean \pm SD), which may have been due to the differential image contrast within the margin of the edematous zone between the two types of imaging sequences. Figure 2 shows an example of the lesion size measurements made via T1- and T2-weighted MRI, along with ATD contours with and without correction for the off-resonance artifacts. The shape of the ATD contours without correction [Fig. 2(c)] showed discontinuities, particularly in the region closest to

the midline (left side of image), which were mainly due to mismatches caused by spatial-shifting artifacts. However, after correction [Fig. 2(d)], the ATD contour shapes more closely resembled the lesion morphology.

Results from the regression and *t*-test analyses are summarized in Table I. The ATD threshold that provided the best correlation (i.e., linear regression slope closest to 1) with the lesion size measured on T2-weighted MRI was 100 CEM [Fig. 3(a), linear regression slope = 0.98, $R^2 = 0.58$], whereas for T1-weighted MRI an ATD value of 200 CEM provided the best correlation [Fig. 3(b), linear regression

slope = 1.00, $R^2 = 0.60$]. On a paired basis, the mean difference between an ATD of 100 CEM and the lesion size measured on T2-weighted MRI was -0.1 mm, with a standard deviation of 0.9 mm. Assuming a normal distribution, 95% of differences were therefore found to lie within 2 standard deviations from the mean (i.e. -0.1 ± 1.8 mm). In other words, the maximum overestimate (underestimate) of the lesion size based on the ATD was 1.7 mm (1.9 mm). Similarly, the mean difference between an ATD of 200 CEM and the lesion size measured on T1-weighted MRI was 0.1 ± 1.6 mm. Logarithmic regressions of lesion sizes measured via T2- and T1-weighted MRI as a function of the ATD are given in Figs. 4(a) and 4(b), respectively. A paired *t*-test failed to reject the null hypothesis that on average an ATD of 100 CEM is equivalent to the lesion size measured on T2-weighted MRI at a significance level of 0.05 ($P = 0.64$). The difference between the mean ATD of 100 CEM and the mean lesion size on T2-weighted MRI ranged from -0.3 mm to 0.2 mm [95% confidence interval (CI)]. Similarly, a paired *t*-test failed to reject the null hypothesis that the mean ATD of 200 CEM is equivalent to the mean lesion size on T1-weighted MRI at a significance level of 0.05 ($P = 0.44$). The difference between the mean ATD of 200 CEM and the mean lesion size on T1-weighted MRI ranged from -0.1 to 0.3 mm (95% CI). A paired *t*-test also failed to reject the null hypothesis for the case of 240 CEM compared with T1-weighted MRI ($P = 0.09$). However, as the regression slope for an ATD of 200 CEM was closer to unity than for the case of 240 CEM (1.00 vs 0.96, respectively), we considered 200 CEM to be a better predictor of the lesion size found on T1-weighted MRI. In contrast, paired *t*-tests for all other CEM values tested in this study (i.e. 17, 40, 200, 240 CEM on T2-weighted MRI, and 17, 40, 100 CEM on T1-weighted MRI) all rejected the null hypotheses with $P < 0.005$ (see Table I).

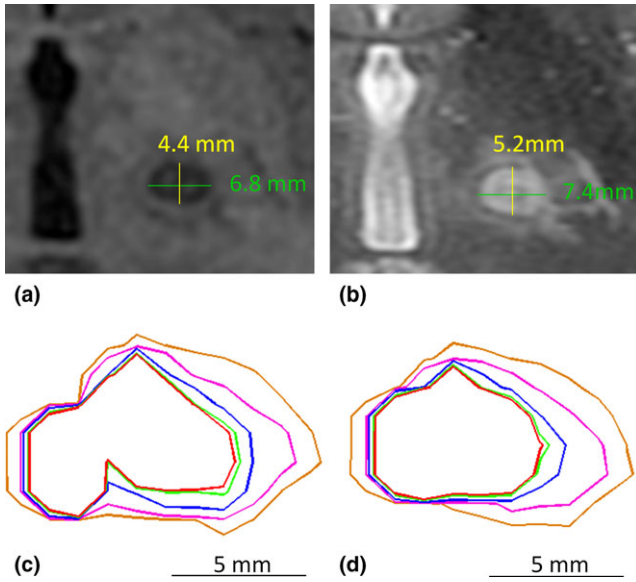


FIG. 2. Example illustrating lesion size and thermal dose measurements. (a). Lesion visualization and size measurement on axial T1-weighted MR imaging; (b). Lesion visualization and size measurement on axial T2-weighted MR imaging; (c). ATD without correction for off-resonance-induced spatial shifts; (d). ATD with correction for off-resonance-induced spatial shifts. The red, light green, blue, pink, and orange contours correspond to regions that received over 240, 200, 100, 40, and 17 CEM, respectively. Nine sonications were used in this calculation, among which six were monitored in axial and three in coronal. [Color figure can be viewed at wileyonlinelibrary.com]

4. DISCUSSION

An earlier report that examined a subset of this clinical data suggested that a thermal dose of 240 CEM

TABLE I. Summary of the regression and paired *t*-test analyses comparing ATD sizes to lesion sizes measured on T1- and T2-weighted MR images.

MRI sequence	ATD (CEM)	Regression slope	Regression R^2	ATD — lesion mean (mm)	ATD — Lesion SD (mm)	<i>t</i> -test <i>P</i> -value	95% CI lower (mm)	95% CI upper (mm)
T1-weighted	17	1.53	0.34	3.0	1.4	<0.005	2.6	3.3
	40	1.32	0.48	1.8	1.0	<0.005	1.5	2.0
	100	1.14	0.54	0.8	0.9	<0.005	0.6	1.0
	200	1.00	0.60	0.1	0.8	0.44	-0.1	0.3
	240	0.96	0.66	-0.1	0.7	0.09	-0.3	0.0
T2-weighted	17	1.33	0.42	2.1	1.3	<0.005	1.8	2.4
	40	1.14	0.54	0.9	1.0	<0.005	0.7	1.2
	100	0.98	0.58	-0.1	0.9	0.64	-0.3	0.2
	200	0.87	0.64	-0.8	0.8	<0.005	-1.0	-0.6
	240	0.84	0.69	-1.0	0.7	<0.005	-1.2	-0.8

R^2 = coefficient of determination, SD = standard deviation, CI = confidence interval.

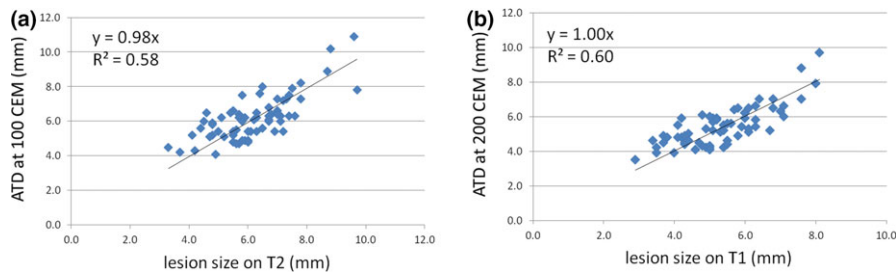


FIG. 3. (a). Linear regression between the lesion size measured on T2-weighted MRI 1 day post-treatment and the size of the ATD profile at 100 CEM; (b). Linear regression between the lesion size measured on T1-weighted MRI 1 day post-treatment and the size of the ATD profile at 200 CEM. The regression slopes were close to unity, indicating a good correlation in both cases. [Color figure can be viewed at wileyonlinelibrary.com]

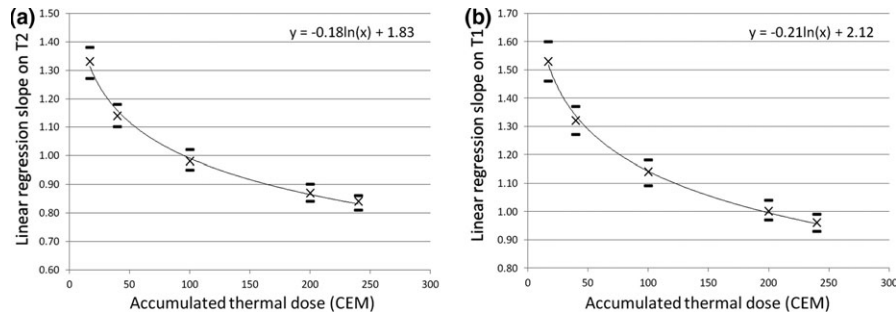


FIG. 4. Slopes of linear regressions between the lesion size measured via (a) T2- and (b) T1-weighted MRI 1 day post-treatment and the ATD profile size for 17, 40, 100, 200, and 240 CEM. Error bars show the range of slope estimates at 95% confidence intervals. Logarithmic regressions showed that the best estimation of the lesion size (i.e. linear regression slope = 1) on T2- and T1-weighted MRI was found using an ATD of 100 and 200 CEM, respectively.

underestimated the size of human brain lesions measured on T1-weighted MRI 1 day post-sonication, whereas 17 CEM tended to overestimate such measurements.¹⁰ However, in that study, only one sonication was considered per patient, namely that which achieved the highest peak temperature throughout the procedure. By accumulating thermal dose profiles from repeated sonications after correcting for off-resonance-induced shifting artifacts, it was found that the thermal dose threshold is in fact closer to 200 CEM [Fig. 4(b)] for these same circumstances (i.e. T1-weighted MRI, 1 day post-sonication). This result is contrary to an earlier preclinical study that reported a thermal dose threshold for brain tissue of approximately 17.5 CEM.⁸ A few technical differences between the current clinical study and that preclinical study might have contributed to this discrepancy; however, it appears that the dominant factor was the different thermal coefficients that were used to calculate the temperature maps in MR-thermometry (clinical study: $-0.00909 \text{ ppm}/^\circ\text{C}$, preclinical study: $-0.011 \text{ ppm}/^\circ\text{C}$). This difference in thermal coefficients led to a 20% difference in the calculated temperature changes between the two studies. For example, a temperature elevation from 37 to 57°C calculated assuming a thermal coefficient of $-0.00909 \text{ ppm}/^\circ\text{C}$ is equivalent to a rise from 37 to 53.5°C with a thermal coefficient of $-0.011 \text{ ppm}/^\circ\text{C}$. Retrospective analysis of our data showed that if the same thermal coefficients are used, an ATD of 200 CEM quoted in this clinical study corresponds to 18 CEM in the pre-clinical work. Prior preclinical studies have estimated the thermal coefficient for both rabbit brain

($-0.0107 \text{ ppm}/^\circ\text{C}$ ¹⁷) and muscle ($-0.00909 \text{ ppm}/^\circ\text{C}$ ^{18,19}). However, the thermal coefficient of human brain is currently unknown due to the lack of analogous calibration data. Regardless, it is important to note that both the temperature and thermal dose data in this study were based on a thermal coefficient of $-0.00909 \text{ ppm}/^\circ\text{C}$, the value currently employed in the clinical MRgFUS brain systems. Thus, if this coefficient is revised in the future, temperature and thermal dose data will need to be revised accordingly.

MRI-based size measurements suggested that, on average, lesions were 15% larger on T2-weighted images than on corresponding T1-weighted images. Previous animal studies have demonstrated correlations between T2-weighted MRI and histology on the central necrosis and surrounding edematous developments over time.²⁰ In addition, signal changes on T1-weighted MRI post-FUS have been correlated with vascular necrosis resulting from thermal coagulation,²¹ which may require higher thermal exposures to induce than the tissue damage indicated by T2-weighted signal changes. It was therefore expected that the ATD threshold that best predicted the lesion size measured on T1-weighted images (200 CEM) could be higher than that for corresponding T2-weighted images (100 CEM), and indeed this was found to be the case in this work.

The off-resonance-induced shifting artifacts observed in this work were largely a result of a mismatch of the center frequencies across the three orthogonal imaging planes caused by differences in magnetic susceptibility from the water volume, and, to a lesser extent, due to heating of the focal

volume.¹¹ Although the magnitudes of the spatial shifts were only about 1–2 mm in most cases, this level of misalignment cannot be ignored when lesions on the order of 5 mm in size are considered. Retrospective realignments of hot spots to the intended target were performed for sonications at therapeutic levels under the assumption that the focal heating volume was properly aligned with the target location during the initial, low-power sonication stage of the procedure. The current MR-thermometry implementation employed a narrow bandwidth (44 Hz/pixel). In the future, the use of a multiecho thermometry sequence that employs multiple high-bandwidth echoes may help minimize off-resonance-induced shifting artifacts.

Although coronal and sagittal thermometry images accounted for only 14% of all sonications included in this study, the transformations from coronal and sagittal images to axial images based on the simplified assumption of an ellipsoidal heating volume may have introduced errors in the calculation of the ATD. However, this was the best possible approximation given the nature of our data, and the resulting errors were assumed to be smaller than those obtained if coronal and sagittal thermometry data were excluded from the dose calculations. Simulations of transcranial acoustic propagation²² could be performed to predict the heating shape in 3D for a given sonication by taking into account the treatment-specific patient positioning and acoustical parameter distributions, however such numerical modeling may induce its own errors and was beyond the scope of the current study. In the future, 3D MR-thermometry²³ could be applied so that the thermal dose can be calculated in all three dimensions simultaneously.

The limitations of this study include potential errors in MR-thermometry, the accuracy in off-resonance shifting correction, uncertainty of the thermal coefficient for human brain tissue, and the fact that only time point (i.e., 1 day post-sonication) was available for measuring the lesion size. The combined impact of these factors was reflected in the relatively low R^2 values obtained from the linear regression analysis and in the relatively large ranges of prediction variability (i.e., ± 1.8 mm for 100 CEM and ± 1.6 mm for 200 CEM). However, to the best of our knowledge, thermal dose thresholds for human brain have yet to be established, due to the lack of *in vivo* data in a more controlled but invasive manner that is possible during preclinical investigations. Therefore, despite the technical limitations of this study, it is the best effort-to-date to establish thermal dose thresholds as a practical guidance for predicting lesion sizes in a clinical setting using the current commercial MRgFUS systems. We anticipate that with further improvements to the MRgFUS system (e.g., higher SNR in MR-thermometry with integrated imaging coils, 3D thermometry for more accurate delineation of the heating volume), the variability of such thermal dose measurements will be reduced in future studies.

In conclusion, using data from patient MRgFUS essential tremor treatments, it was demonstrated that the ATD is correlated with the lesion size measured via MRI 1 day post-sonication. The ATD thresholds that were the best predictors of

the lesion size on T1- and T2-weighted images were 200 and 100 CEM, respectively. These data provide information that is useful for predicting lesion size and determining treatment endpoints in the future clinical MRgFUS thalamotomy for essential tremor.

ACKNOWLEDGMENTS

The authors thank Xinhao Zhang for software programming in MATLAB™ related to the ATD quantification. Support for this work was provided by the National Institutes of Health under grant number R01-EB003268 and the Canada Research Chairs Program.

CONFLICT OF INTEREST

The authors have no relevant conflicts of interest to disclose.

^{a)}Author to whom correspondence should be addressed. Electronic mail: huangyx@sri.utoronto.ca; Telephone: + 416-480-6156.

REFERENCES

1. Elias WJ, Lipsman N, Ondo WG, et al. A randomized trial of focused ultrasound thalamotomy for essential tremor. *N Engl J Med.* 2016;375:730–739.
2. Lipsman N, Schwartz ML, Huang Y, et al. MR-guided focused ultrasound thalamotomy for essential tremor: a proof-of-concept study. *Lancet Neurol.* 2013;12:462–468.
3. Elias WJ, Huss D, Voss T, et al. A pilot study of focused ultrasound thalamotomy for essential tremor. *N Engl J Med.* 2013;369:640–648.
4. Chang WS, Jung HH, Zadicario E, et al. Factors associated with successful magnetic resonance-guided focused ultrasound treatment: efficiency of acoustic energy delivery through the skull. *J Neurosurg.* 2016;124:411–416.
5. McDannold N, King RL, Jolesz FA, et al. Usefulness of MR imaging-derived thermometry and dosimetry in determining the threshold for tissue damage induced by thermal surgery in rabbits. *Radiology.* 2000;216:517–523.
6. Schuurman PR, Bosch DA, Merkus MP, et al. Long-term follow-up of thalamic stimulation versus thalamotomy for tremor suppression. *Mov Disord.* 2008;23:1146–1153.
7. Wintermark M, Druzgal J, Huss DS, et al. Imaging findings in MR imaging-guided focused ultrasound treatment for patients with essential tremor. *Am J Neuroradiol.* 2014;35:891–896.
8. McDannold N, Vykhodtseva N, Jolesz FA, et al. MRI investigation of the threshold for thermally induced blood-brain barrier disruption and brain tissue damage in the rabbit brain. *Magn Reson Med.* 2004;51:913–923.
9. Yarmolenko PS, Moon EJ, Landon C, et al. Thresholds for thermal damage to normal tissues: an update. *Int J Hyperthermia.* 2011;27:320–343.
10. Huang Y, Lipsman N, Schwartz ML, et al. Correlation of Lesion Size to Thermal Dose Measured by MR Thermometry in MR-Guided Focused Ultrasound for the Treatment of Essential Tremor. Poster session presented at 23rd Scientific Meeting of the International Society for Magnetic Resonance in Medicine; 2015 Jun 1-5; Toronto, Canada.
11. Gaur P, Partanen A, Werner B, et al. Correcting heat-induced chemical shift distortions in proton resonance frequency-shift thermometry. *Magn Reson Med.* 2016;76:172–182.
12. McDannold N, Clement GT, Black P, et al. Transcranial magnetic resonance imaging-guided focused ultrasound surgery of brain tumors: initial findings in 3 patients. *Neurosurgery.* 2010;66:323–332.

13. Yoshida M. Neurophysiological atlas created by mapping of clinical responses elicited on electrical stimulation of the human thalamus. *Stereotact Funct Neurosurg.* 1992;58:39–44.
14. Moser D, Zadicario E, Schiff G, et al. Measurement of targeting accuracy in focused ultrasound functional neurosurgery. *Neurosurg Focus.* 2012;32:E2.
15. Sapareto SA, Dewey WC. Thermal dose determination in cancer therapy. *Int J Radiat Oncol Biol Phys.* 1984;10:787–800.
16. Dewhurst MW, Viglianti BL, Lora-Michiels M, et al. Basic principles of thermal dosimetry and thermal thresholds for tissue damage from hyperthermia. *Int J Hyperthermia.* 2003;19:267–294.
17. Vykhodtseva N, Sorrentino V, Jolesz FA, et al. MRI detection of the thermal effects of focused ultrasound on the brain. *Ultrasound Med Biol.* 2000;26:871–880.
18. McDannold N. Quantitative MRI-based temperature mapping based on the proton resonant frequency shift: review of validation studies. *Int J Hyperthermia.* 2005;21:533–546.
19. Chung AH, Jolesz FA, Hynynen K. Thermal dosimetry of a focused ultrasound beam in vivo by magnetic resonance imaging. *Med Phys.* 1999;26:2017–2026.
20. Morocz IA, Hynynen K, Gudbjartsson H, et al. Brain edema development after MRI-guided focused ultrasound treatment. *J Magn Reson Imaging.* 1998;8:136–142.
21. Hynynen K, Darkazanli A, Damianou CA, et al. The usefulness of a contrast agent and gradient-recalled acquisition in a steady-state imaging sequence for magnetic resonance imaging-guided noninvasive ultrasound surgery. *Invest Radiol.* 1994;29:897–903.
22. Pulkkinen A, Werner B, Martin E, et al. Numerical simulations of clinical focused ultrasound functional neurosurgery. *Phys Med Biol.* 2014;59:1679–1700.
23. Todd N, Vyas U, de Bever J, et al. Reconstruction of fully three-dimensional high spatial and temporal resolution MR temperature maps for retrospective applications. *Magn Reson Med.* 2012;67:724–730.